*Nonlinear Processes in Geophysics*

Supporting Information for

# Targeted Adaptive Chaos Control of Regimes and Eddy Strength in Two Lorenz Models

Moyan Liu[1], Qin Huang[1], Upmanu Lall[1,2*]

[1]School of Complex Adaptive Systems & Water Institute, Arizona State University, Tempe, AZ, 85281, USA.
[2]Department of Earth and Environmental Engineering & Columbia Water Center, Columbia University, New York, 10025, NY, USA.

*Correspondence to*: Upmanu Lall (ulall@asu.edu)

## Contents of this file



## Introduction

This supporting information contains details on how we construct and evaluate a data-driven surrogate model for the Lorenz 63 (L63) and Lorenz 84 (L84) systems (Text S1), and how we assess the short-term forecast accuracy of the surrogate dynamics using polynomial ridge regression. Supporting figures (Figures S1–S7) illustrate the accuracy of surrogate models (S1–S2), successful control of the L63 trajectory in 2D (S3), the impact of LLE thresholds on control effectiveness and energy cost (S4), the relationship between eddy amplitude and instability (S5), spatial localization of high eddy activity in the L84 attractor (S6), and the control-to-total energy ratio over time in the L84 scenario (S7).

**Text S1. Surrogate Model Construction**

To approximate the Lorenz dynamical systems, we construct a surrogate model using polynomial feature expansion and ridge regression, trained on trajectory data generated from the Lorenz 63 (L63) and Lorenz 84 (L84) models. Trajectory data were generated using a 4th-order Runge-Kutta with a time step of $\Delta t=0.01$, yielding both system states and their time derivatives. Specifically, we use second-degree polynomial ridge regression to approximate the local vector field, i.e., the time derivative of the system state. The polynomial terms capture key nonlinear interactions among the state variables, while ridge regularization mitigates overfitting to local noise and high-frequency fluctuations. The surrogate model takes the form:

$$\hat{f}(\mathbf{x}) = \mathbf{W}^* \cdot \Phi(\mathbf{x})$$

where $\Phi(x)$ is the second-degree polynomial feature vector and $W^*$ is obtained by minimizing the regularized squared loss:

$$\mathbf{W}^* = \arg\min_{\mathbf{W}} \left\| \Phi\mathbf{W} - \dot{X} \right\|_2^2 + \alpha \left\| \mathbf{W} \right\|_2^2$$

with regularization parameter $\alpha = 10^{-6}$. This surrogate is then used to propagate future states using a 4th-order Runge-Kutta scheme, enabling fast forecasting and gradient-based control optimization.

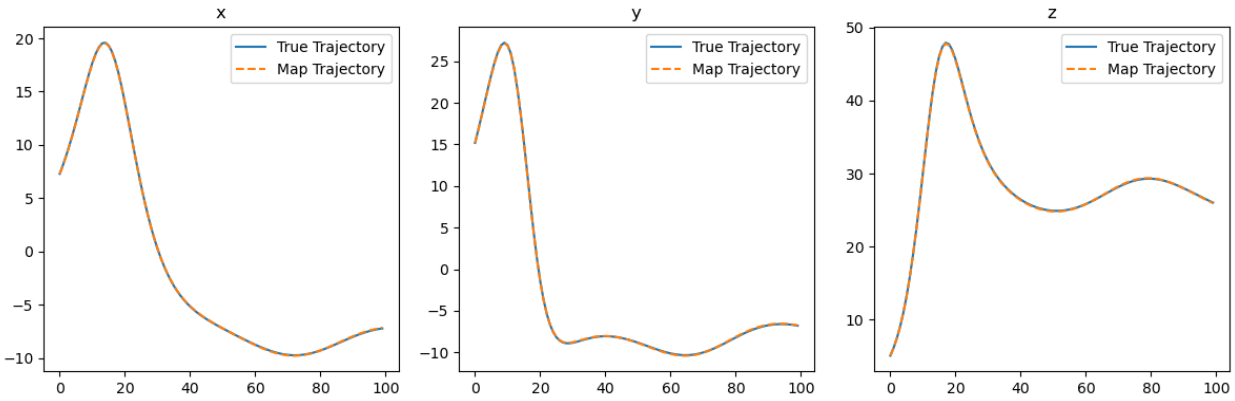


**Figure S1.** Comparison between the true L63 trajectory and the surrogate model trajectory over a 100-step forecast horizon. Gaussian noise was added to the forecast at each step. The mean squared error (MSE) between the true and surrogate trajectories is 0.003. Our typical forecast window for control experiments is approximately 10 steps, indicating that the surrogate model achieves sufficient accuracy for short-term prediction tasks.

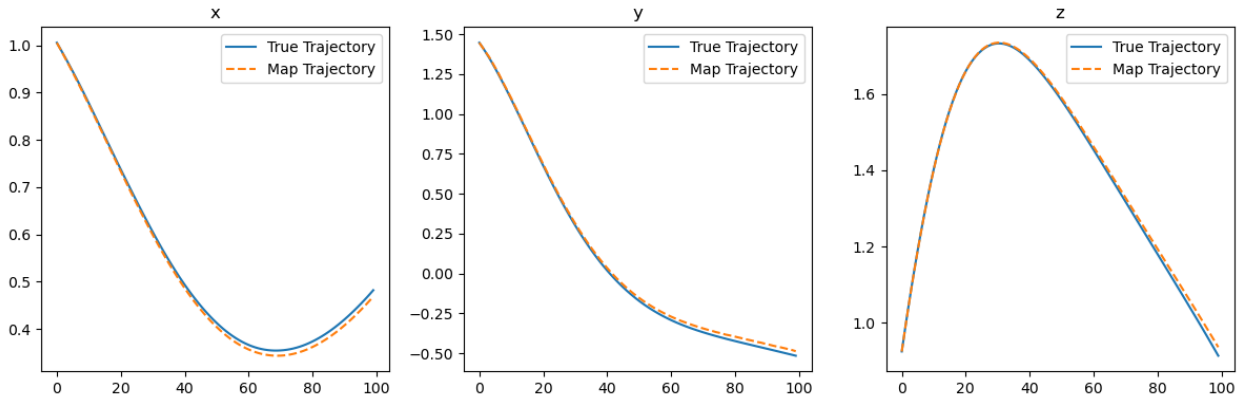


**Figure S2.** Comparison between the true L84 trajectory and the surrogate model trajectory over a 100-step forecast horizon. Gaussian noise was added to the forecast at each step. The mean squared error (MSE) between the true and surrogate trajectories is 0.0002. Our typical forecast window for control experiments is approximately 10 steps, indicating that the surrogate model achieves sufficient accuracy for short-term prediction tasks.

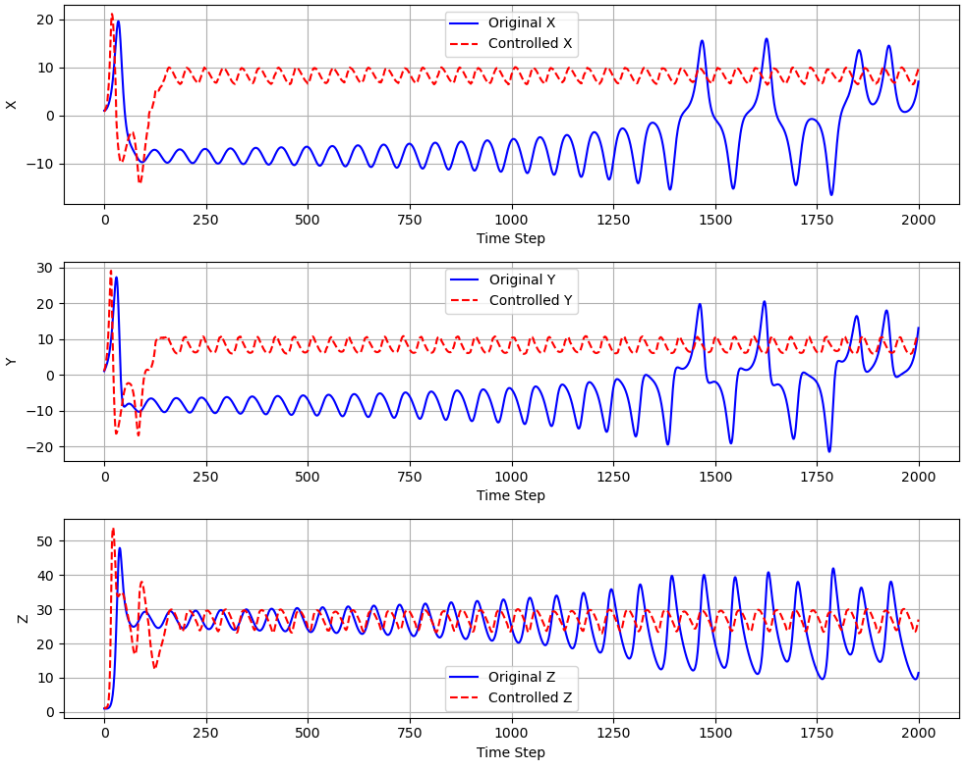


**Figure S3.** 2D projection of controlled and natural trajectories of the L63 model in the x, y, z axis with time steps. The controlled trajectory remains confined to one side of the attractor, demonstrating suppression of regime shifts.

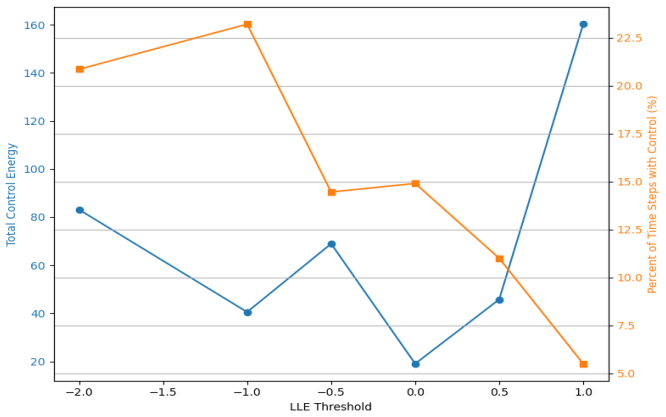


**Figure S4.** Trade-off between total control energy (blue, left axis) and percentage of time steps with control applied (orange, right axis) as a function of LLE threshold.

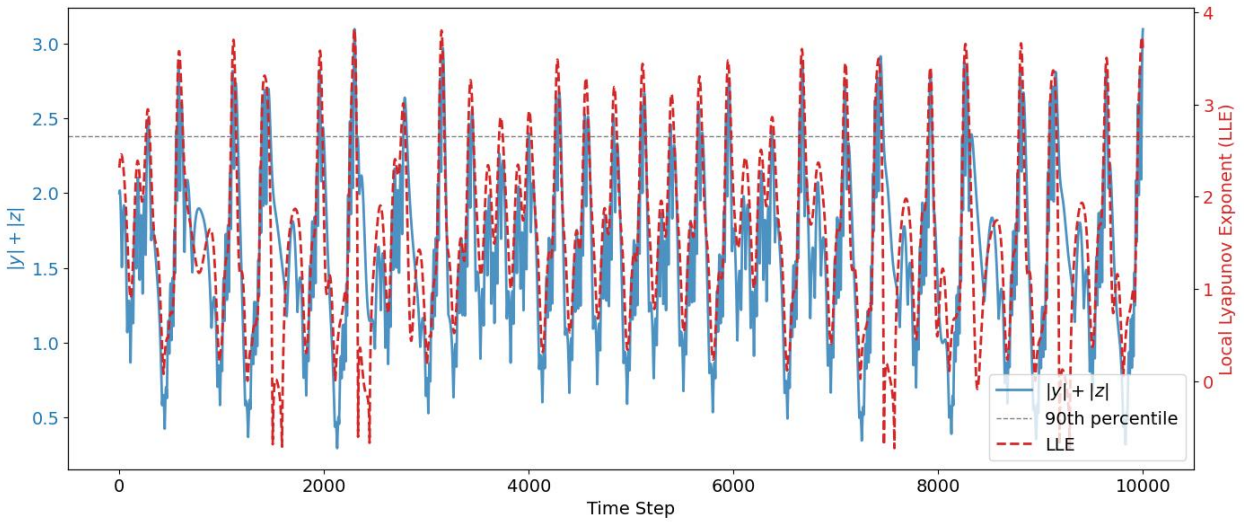


**Figure S5.** Time series of combined eddy amplitude (|Y|+|Z|, blue) and local Lyapunov exponent (LLE, red dashed) over simulation time steps for the L63 system. The horizontal dashed gray line marks the 90th percentile threshold of |Y|+|Z|, used to identify high eddy activity. The plot illustrates the temporal correspondence between elevated eddy amplitudes and local instability, supporting the control strategy based on eddy suppression.

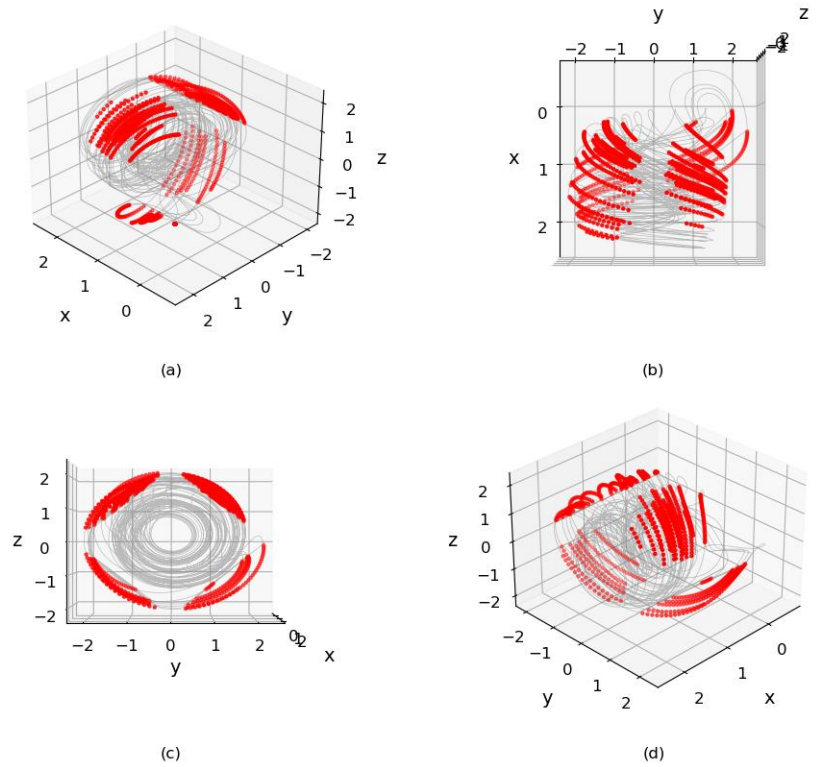


**Figure S6.** Multiple views of the L84 trajectory, with high eddy activity highlighted in red. The gray line represents the full trajectory, while red markers indicate time steps where the combined eddy amplitude (|Y|+|Z|) exceeds a prescribed threshold. Subfigures show different perspectives:(a) default 3D view, (b) view in the x-y plane, (c) view in the y-z plane, and (d) an alternate 3D perspective. These views help visualize the spatial distribution and localization of high eddy regions within the attractor.

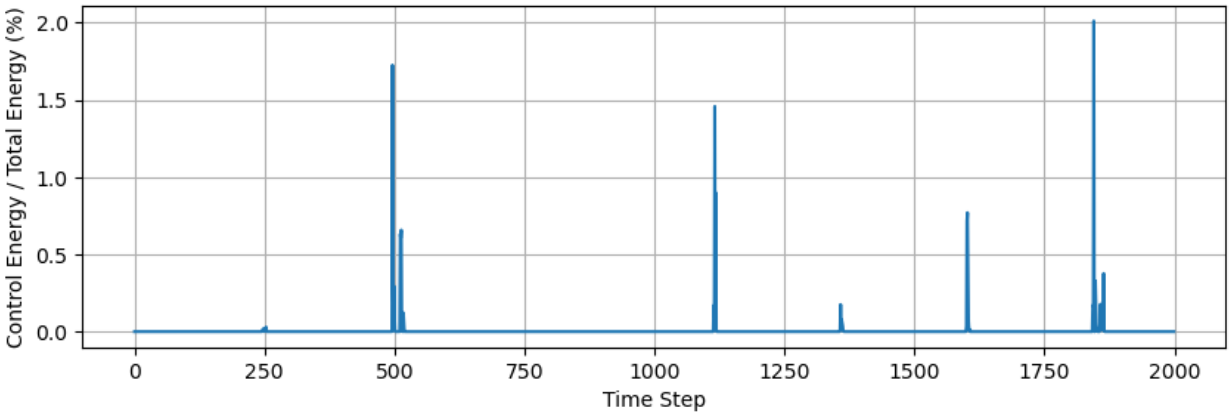


**Figure S7.** Ratio of control energy to total system energy over time in the L84 control scenario.